Near-Surface Electronic Contribution to Semiconductor Elasticity

J. T. Lin,[1] P. D. Shuvra,[1] S. McNamara,[1] H. Gong,[2] W. Liao,[2] J. L. Davidson,[2] K. M. Walsh,[1] M. L. Alles,[2] and B. W. Alphenaar[1,*]

[1]*Department of Electrical and Computer Engineering, University of Louisville, Louisville, Kentucky 40292, USA*

[2]*Department of Electrical Engineering and Computer Science, Vanderbilt University, Nashville, Tennessee 37235, USA*

(Received 5 January 2017; revised manuscript received 13 July 2017; published 18 September 2017)

The influence of the carrier concentration on the elasticity is measured for a microscale silicon resonator. UV radiation is used to generate a surface charge that gates the underlying carrier concentration, as indicated by the device resistance. Correlated with the carrier concentration change is a drop in the resonant frequency that persists for 60 h following exposure. Model calculations show that the change in resonant frequency is due to the modification of the elastic modulus in the near-surface region. This effect becomes increasingly important as device dimensions are reduced to the nanometer scale, and contributes an important source of instability for microscale and nanoscale electromechanical devices operating in radiation environments.

DOI: 10.1103/PhysRevApplied.8.034013

I. INTRODUCTION

Microelectromechanical systems (MEMS) functioning as oscillators, accelerometers, gyroscopes, and seismometers have clear advantages over traditional sensing and timing technology for space-based applications [1–4]. They are small, lightweight, capable of being integrated with silicon ICs, and use low power. These advantages are of particular importance for "picosatellite" applications [5,6], where stringent size and weight limitations exist. Essential for any MEMS space-based application is an understanding of the impact that high radiation environments encountered in space have on MEMS operation. Studies of radiation effects on commercially available MEMS components have described the impact that radiation-induced electrostatic charging has on MEMS operation [7,8]. A number of optomechanical studies have also been reported on the interaction of pulsed laser light with nanoscale mechanical resonators [9–15]. High-speed optical excitation of charge carriers can induce mechanical oscillations, and alter mechanical resonant amplitudes. Nonradiative carrier recombination causes local heating, which also temporarily modifies the resonant frequency. These works clearly demonstrate the impact of optically induced charge generation on material mechanical properties, however, these effects dissipate quickly once the pulsed laser light is removed.

Recently, our group showed how x-ray radiation causes long-term changes to the elastic properties of silicon MEMS cantilevers [16,17]. It was proposed that the modification was due to the depassivation of bound hydrogen-boron pairs by the x-ray radiation. This releases holes, raising the carrier concentration and reducing the elastic modulus. The observed effects are dependent on the relationship between semiconductor carrier concentration and mechanical properties, as first described by Keyes [18]. Mechanical strain causes the electronic energy bands to shift, redistributing the available electron states. This modifies the free energy by an amount that is dependent on the concentration of carriers available for redistribution. This results in an additional electronic contribution to the elasticity that should be observable as a carrier-concentration dependence in the Young's elastic modulus [19]. Semiconductors with different dopant concentrations have been observed to have different Young's modului [20], in rough agreement with Keyes' theory. However, direct measurements of the carrier-concentration-dependent Young's modulus have not been made. Surface charging can produce large changes in the near-surface carrier concentration due to band bending, that might also be expected to change the near-surface elastic constants. In macroscale samples, the influence of the surface on the elastic constants is negligible; however, it becomes increasingly important as device dimensions decrease into the microscale and nanoscale regimes [21].

In this paper, we explore how ultraviolet (UV) radiation influences the elastic properties of a microscale silicon resonator. UV radiation differs from x-ray radiation in that the penetration depth is much lower (<15 nm), so that any observed changes should be due to the impact of the UV radiation on the near-surface region. UV-induced changes in the carrier concentration are detected using four-terminal resistance measurements. Simultaneously monitoring the resonant frequency of the resonator shows that the Young's

*brucea@louisville.edu

modulus decreases as the carrier concentration increases, clearly demonstrating the impact of the free carrier concentration on the elasticity, independent of dopant concentration. Theoretical modeling shows that the impact of the surface carrier concentration on the elasticity increases dramatically as the surface-to-volume ratio of the resonator increases, implying that nanoscale electromechanical systems will be highly susceptible to near-surface carrier-concentration-induced changes to the Young's modulus.

II. EXPERIMENTAL PROCEDURE

Figure 1 shows the device layout and experimental setup. The starting material for the resonator is a silicon-on-insulator wafer with a device-layer thickness of 15 μm, a buried oxide layer thickness of 2 μm, and a handle layer thickness of 500 μm. The device layer is boron doped (p-type) to a resistivity of approximately 0.013 Ω cm. T-shaped cantilevers are defined in the device layer using the deep reactive-ion etching process, and then released from the backside by subsequent dry etching. Prior to measurement, the sample chamber is evacuated using a turbomolecular pump. The chamber is pumped for 72 h, until the pressure is constant as measured at the pump inlet. The cantilever beam is actuated by an ac voltage on a nearby gate electrode, and is continuously driven during the course of the measurement.

The resistance of the base changes with the strain of the moving cantilever due to the piezoresistivity of the silicon, so that cantilever motion can be detected by monitoring the ac voltage generated across a sense resistor in series with the base. The base has an asymmetric design to maximize the resistance change [22]. Figure 1(b) shows the frequency response of a representative device measured in a vacuum chamber at a pressure of 2×10^{-6} mbar. A peak is observed at a frequency of 21.307 kHz; high-speed camera imaging confirms that this peak correlates with the cantilever resonance. In subsequent measurements, the resonant frequency of the cantilever and the four-terminal resistance of the base are monitored while the sample is exposed to light through a quartz window in the vacuum chamber. For reference, a second resonator is placed adjacent to the test device, but shielded from the light by a metal plate [see Fig. 1(c)]. Comparison between the exposed and unexposed samples allows for changes due to carrier generation to be isolated from those due to temperature.

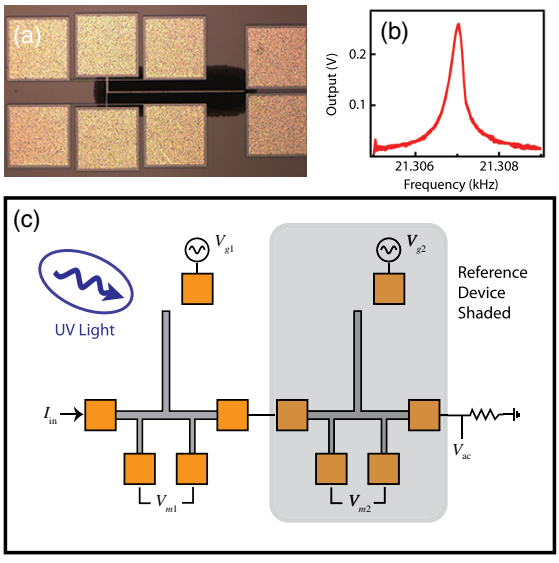

FIG. 1. (a) Optical microscope image of the resonator. The resonator beam is 655 μm long, 8 μm wide, and 15 μm thick. The voltage contacts on the base are separated by 110 μm. (b) Output versus driving frequency for a representative device. Nine different scans are plotted together to demonstrate the device reproducibility. (c) Schematic showing the measurement configuration. The asymmetric base is not shown.

III. DEVICE MEASUREMENTS

As an initial demonstration of the measurement technique, the resonator is exposed to blue light of energy below the oxide band edge. The blue light source is an Engin LZ1-10D800 LED with a peak wavelength of 425 nm and a measured output power of 1.44 mW. Figure 2 shows the (a) four-terminal resistance and (b) resonant frequency plotted as a function of time before, during, and after a 30-min exposure to light from the 465-nm LED. The resistance increases and the resonant frequency decreases during exposure, with a similar change being observed in both shielded and unshielded devices. It is known that the silicon hole mobility and Young's

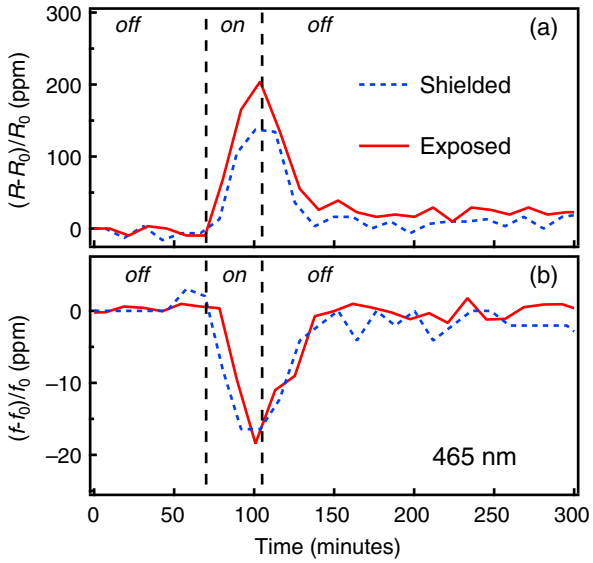

FIG. 2. (a) Change in the four-terminal resistance of the resonator beam and (b) change in the resonant frequency, for samples exposed and shielded from 465-nm blue light.

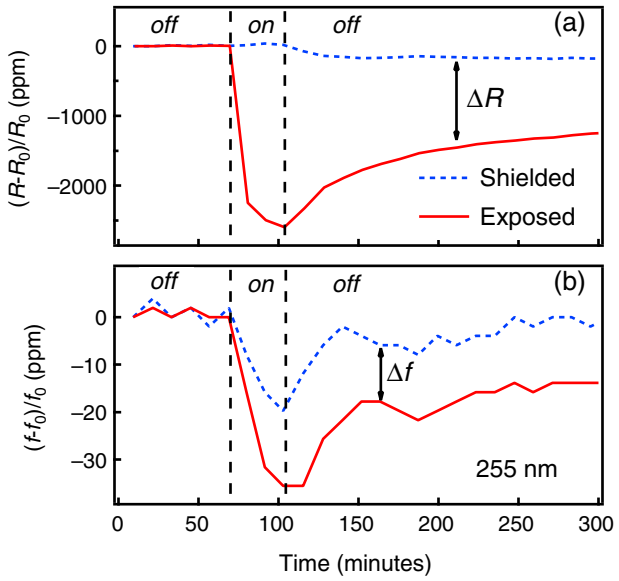

FIG. 3. (a) Change in the four-terminal resistance of the resonator beam and (b) change in the resonant frequency, for samples exposed and shielded from 255-nm UV light.

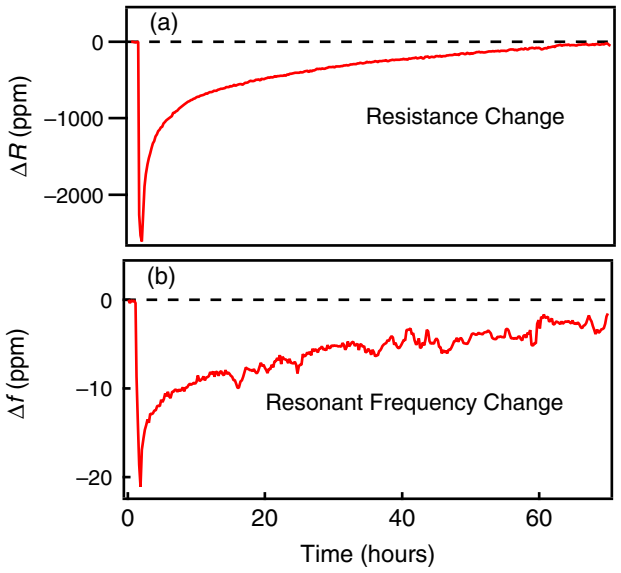

FIG. 4. Difference between (a) the four-terminal resistance ΔR and (b) the resonant frequency Δf for the exposed sample and reference sample measured as a function of time following a 30-min exposure to 255-nm light.

modulus both decrease with increasing temperature, so that the observed changes can be attributed to heating of the sample chamber. Once the light is removed, the original signal is recovered in approximately 20 min, providing a measure of the thermal recovery time for the resonator. By comparison, Fig. 3 shows the impact that UV light from a 255-nm LED has on (a) the four-terminal resistance and (b) the resonance frequency. The UV source is a Thorlabs LED255J Optan UV LED with measured output power of 220 μW. The shielded device is now used to monitor the heating caused by the UV light; its resistance increases and resonant frequency decreases as before, and both recover in approximately 20 min following exposure. The exposed sample behaves very differently. Its resistance drops a large amount (rather than rising), while the resonant frequency drops below the reference value of the shielded device. Neither recover back to their original values over the 300-min measurement.

The difference in signal between the shielded and exposed devices gives the change due to the UV light that is not due to heating. This is plotted as a function of time in Fig. 4 for the (a) resistance ΔR and for the (b) resonance frequency Δf. Both drop sharply following UV exposure, and then slowly recover back to their original values over approximately 60 h. The similarity between the resistance recovery and the resonance frequency recovery suggests that the two are related, even though the total resistance change (2500 ppm) is 100 times larger than the total frequency change (25 ppm). Further analysis shows that the resistance and resonant frequency recover to their equilibrium values logarithmically with time, as is observed for many slow relaxation processes [23]. Measurements are repeated for five different sets of samples, and in each case, similar results are observed.

IV. DISCUSSION AND THEORETICAL MODEL

The effect of UV light on a silicon surface has been described in detail in the literature [24–26]. UV light is absorbed in the near-surface region (with an absorption depth of 10 nm for 255-nm light). This creates highly excited electron-hole pairs with energies above the conduction and valence bands of the overlying native silicon oxide layer. Some amount of the excited charge Q_{ox} is transferred to the oxide, where it becomes trapped. Photovoltage [27] and second-harmonic generation experiments [28] have shown that the trapped oxide charge has an extremely long lifetime, and slowly decays over a period of two-to-three days following UV exposure. The surface oxide charge is balanced by an equal but opposite charge due to the accumulation or depletion of carriers in the underlying silicon. In the following, it is shown that this change in surface carrier concentration can account for our experimentally observed behavior: the resistance of the silicon drops due to carrier-concentration dependence of the conductivity, and the resonance frequency drops due to the carrier-concentration dependence of the Young's modulus.

A. Resistance calculation

The first step in the resistance calculation is to determine the carrier concentration as a function of distance from sample surface x. From standard semiconductor theory

[29], the following relationship holds for the potential in the silicon $\phi(x)$:

$$\frac{\partial\phi(x)}{\partial x} = -\left(\frac{2kTp_0}{\epsilon}\right)^{1/2}\left[\left(e^{-[q\phi(x)]/kT} + \frac{q\phi(x)}{kT} - 1\right) + \frac{n_0}{p_0}\left(e^{[q\phi(x)]/kT} - \frac{q\phi(x)}{kT} - 1\right)\right]^{1/2} = g(\phi(x)), \quad (1)$$

where q is the charge, k is Boltzman's constant, T is the temperature, ϵ is the silicon dielectric constant, and n_0 and p_0 are the equilibrium electron and hole concentrations in the bulk of the sample. Here, the function $g(\phi(x))$ has been introduced as shorthand for the right-hand side of the equation.

Using Eq. (1) and the relationship $Q_{\rm ox} = \epsilon d\phi_s/dx$, the value of the surface potential ϕ_s can be determined as a function of $Q_{\rm ox}$. Equation (1) is then rewritten through the separation of variables and integration to give

$$x = \int_{\phi_s}^{\phi(x)} \frac{d\phi(x')}{g(\phi(x'))} \quad (2)$$

Equation (2) is solved numerically to determine the relationship between $\phi(x)$ and distance x using the value of ϕ_s that corresponds to the chosen $Q_{\rm ox}$. The hole and electron concentrations as a function of distance can then be calculated using

$$p(x) = p_0 \exp\left(\frac{-q\phi(x)}{kT}\right), \qquad n(x) = \frac{n_i^2}{p(x)}.$$

Figure 5 shows the (a) electron concentration and (b) hole concentration as a function of distance from the sample surface, for three different oxide charge concentrations. Reasonable magnitude variations in the oxide charge (on the order of 10^{13} cm^2), causes the silicon surface region to vary between accumulation, depletion, and strong inversion.

To determine the change in resonator base resistance, the base cross section is divided into two regions (see inset to Fig. 6): an outer surface region, with variable carrier concentration and conductivity σ, and an inner region, with carrier concentration and conductivity set to the bulk values. The width of the outer region is determined by the maximum depletion layer width, which as seen in Fig. 5 is approximately 20 nm. The mobility is assumed to be constant and equal to its bulk value throughout the entire sample [30]. The resistance is then determined using $R = L_b/\int_S \sigma dS$, where L_b is the length of the resonator base, and the conductivity is integrated over the base cross section. Figure 6 shows the change in resistance from the flatband condition as a function of oxide charge density. Negative oxide charge results in the accumulation of holes and a decrease in resistance, while positive oxide charge depletes holes and increases the resistance. Very high positive oxide charge concentration inverts the surface carrier concentration, and the resistance again decreases. The calculation shows that a change in oxide charge

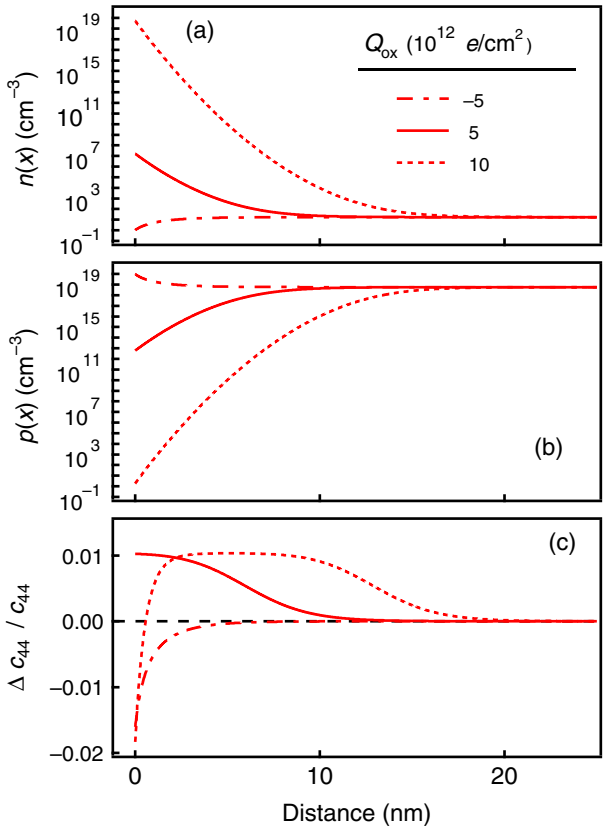

FIG. 5. (a) Electron concentration $n(x)$, (b) hole concentration $p(x)$, and (c) relative shear elastic constant $\Delta c_{44}(x)/c_{44}$ as a function of distance from the sample surface plotted for three different oxide charge concentrations.

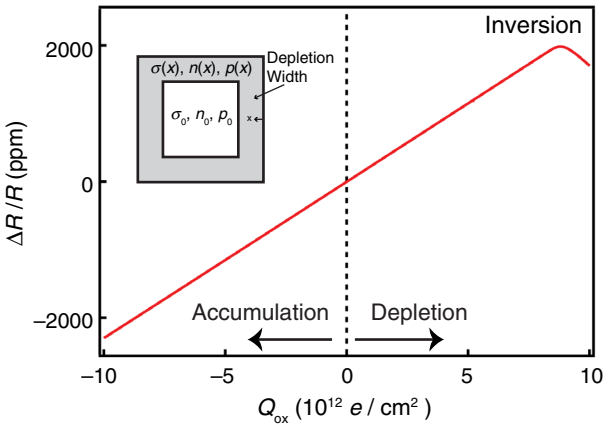

FIG. 6. Relative change in resistance as a function of oxide charge concentration calculated using the model described in the text. The inset shows a cross section of the beam indicated the different regions used in the calculation.

concentration of about -10^{13} cm^{-2} (e.g., from 5×10^{12} cm^{-2} to -5×10^{12} cm^{-2}) reduces the resistance by the experimentally observed value of 2500 ppm.

B. Resonant frequency calculation

Next, consider the influence of the surface oxide charge on the resonant frequency. It is known that a dc electric field between the beam and gate can reduce the resonant frequency due to "spring softening" [31]. In our device, the oxide charge is screened by the highly doped silicon, so that the field outside of the silicon surface is extremely small. In addition, the distance between the beam and the gate is relatively large. Calculations of the resonant frequency shift due to spring softening are performed [32,33] and show that the predicted resonant frequency change is an order of magnitude smaller than that observed experimentally. We have also considered the possibility that the mass of the resonator changes due to surface adsorbants generated by the UV exposure. Calculations show that the observed 20-ppm resonant frequency shift would require the deposition of eight monolayers of nitrogen on the cantilever surface [32]. It is unlikely that multiple atomic layers would remain stable on the cantilever following UV exposure. In addition, atomic adsorption is expected to affect both shielded and unshielded devices equally. Note that deadsorption from the cantilever, while more plausible, would cause the resonant frequency to go up, in disagreement with the observed results.

Instead, consider the effect that the surface carrier concentration has on the resonant frequency. Once again, the beam is taken to be composed of two regions: a bulk region where the shear modulus c_{44} is constant, and a surface region where the shear modulus $c_{44}-\Delta c_{44}(x)$ varies as a function of distance x from the sample surface due to the changing carrier concentration. According to models by Keyes [34] and Einspruch and Csavinsky [35] the change in the shear elastic constant $\Delta c_{44}[n(x)]$ due to the electron concentration $n(x)$ and $\Delta c_{44}[p(x)]$ due to the hole concentration $p(x)$ is given by

$$\Delta c_{44}[n(x)] = -\frac{4}{3}\left(\frac{4\pi}{3}\right)^{2/3}\left(\frac{m_n\Xi^2 n(x)^{1/3}}{h^2}\right), \quad (3a)$$

$$\Delta c_{44}[p(x)] = -\frac{1}{5}\left(\frac{8\pi}{3}\right)^{2/3}\left(\frac{m_p\Xi^2 p(x)^{1/3}}{h^2}\right), \quad (3b)$$

where m_n is the effective electron mass, m_p is the effective hole mass (assuming a nonparabolic heavy hole mass), Ξ is the deformation potential (taken to be 5.5 eV for electrons and 13.8 eV for holes), and $\Delta c_{44}=\Delta c_{44}(n)+\Delta c_{44}(p)$ is the change in c_{44} from its value in intrinsic silicon (79.51 GPa). The substrate used in this work is heavily doped with $N_A=5.8\times10^{18}$ cm^{-3}, so according to Eq. 3(b), c_{44} in the bulk of the sample is equal to 78.69 GPa. Figure 5(c) then shows the change in c_{44} from this bulk value as a function of distance x from the sample surface calculated using Eq. (3) and incorporating the variation in carrier concentration due to band bending shown in Figs. 5(a) and 5(b). The shear elastic constant changes by as much as 2% near the sample surface, recovering to its bulk value over a distance of about 20 nm.

Using the surface-modified elastic constant, the change in the beam resonant frequency is calculated as follows. First, the Young's modulus E is taken to be approximately equal to the shear elastic constant c_{44} (this is reasonable in the experimental beam geometry, where beam motion is mainly in the [110] direction). Next, following the method described in Ref. [36], the beam cross section is transformed into an equivalent shape with a constant elastic modulus. The moment of inertia I is then determined for the transformed geometry, and the resonant frequency calculated using

$$\omega = \left(\frac{\xi^*}{L}\right)^2\sqrt{\frac{EI}{\rho A}} \quad (4)$$

taken from standard beam theory. Here, L is the beam length, A is the cross-sectional area, ρ is the silicon density, and $\xi^*=1.875\,104$ from $1+\cos\xi^*\cosh\xi^*=0$. The results of this calculation are shown in Fig. 7, where the normalized change in resonant frequency is plotted as a function of oxide charge density. The model predicts that a change in oxide charge density of -10^{13} cm^{-2} (as is needed to produce the resistance change in Fig. 6) produces a decrease in resonant frequency close to the experimentally observed value of 25 ppm. The total change in resonant frequency will depend on the initial charge concentration. Note also that the photon energy of the UV light is large

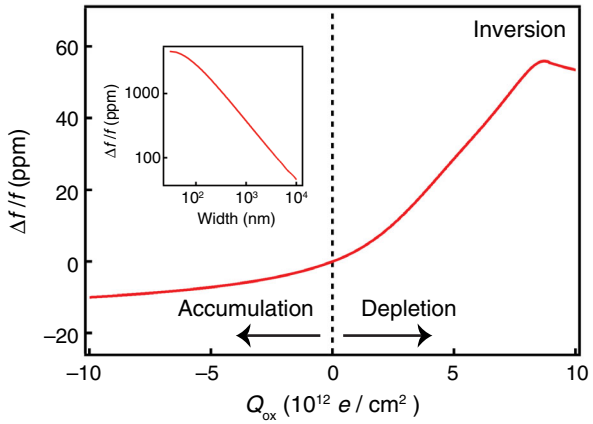

FIG. 7. Relative change in resonant frequency as a function of oxide charge calculated using the model described in the text. The inset shows the relative change in resonant frequency as a function of beamwidth plotted on a log-log scale. The oxide charge is taken to be $Q_{ox}=8.71\times10^{13}\ e/\text{cm}^2$.

enough to produce additional carriers through the boron depassivation mechanism described in Ref. [17], so it is possible that this mechanism also plays a role in modifying the carrier concentration, at least in the near-surface region where the UV light is absorbed.

The impact of the surface oxide charge on the resonant frequency, while clearly detected, is relatively small for this microscale cantilever beam. As the device dimensions decrease and the surface-to-volume ratio increases, the impact of surface charging will also increase. The inset to Fig. 7 shows the maximum calculated change in resonant frequency due to an increase in surface oxide charge of 8.7×10^{12} cm^{-2} as a function of the cantilever beamwidth. The resonant frequency change increases rapidly with decreasing dimensions, and is greater than 3000 ppm for sub-100-nm-width beams. This is a substantial amount for MEMS oscillator applications where 1–10 ppm stability is desirable in order to substitute for quartz crystals in commercial applications [37]. The effects we describe are demonstrated for UV light, however, they would also occur for any type of radiation (gamma rays, high-energy protons) with energy above the Si/SiO_2 energy barrier. UV radiation can be easily blocked with a lightweight shield, but blocking space radiation requires a large amount of mass, negating the advantages of lightweight MEMS technology [7]. The change in resonant frequency eventually saturates with constant UV exposure, however, exposure to high-energy radiation would generate more surface states, making the resonator progressively more susceptible to radiation damage [38]. Radiation-induced changes in mechanical properties due to carrier concentration changes would be particularly important in materials that exhibit persistent photoconductivity. This includes many compound semiconductors (including GaN and ZnO) [39,40] amorphous silicon [41], and semiconductor nanostructures and membranes [42]. It is also noted that the instabilities and electric field-induced shifts reported in the literature for nanometer-scale resonators could in part be attributable to surface carrier concentration changes [43,44].

V. CONCLUSION

In conclusion, the electronic contribution to the silicon elastic properties is measured for a microscale resonator beam, independent of dopant concentration. Changes in the shear elastic modulus with carrier concentration on the sample surface can account for an observed change in resonant frequency following UV exposure. Calculations show that these changes become increasingly important as the sample size is reduced, and could constitute an important drift mechanism for MEMS or NEMS resonators operating in high radiation environments.

ACKNOWLEDGMENTS

Funding was provided by DTRA-HDTRA1-15-1-0027.

[1] J. W. Judy, Microelectromechanical systems (MEMS): Fabrication, design and applications, Smart Mater. Struct. **10**, 1115 (2001).
[2] R. Osiander, S. L. Firebaugh, J. L. Champion, D. Farrar, and M. A. G. Darrin, Microelectromechanical devices for satellite thermal control, IEEE Sens. J. **4**, 525 (2004).
[3] X. Lafontan, F. Pressecq, F. Beaudoin, S. Rigo, M. Dardalhon, J. L. Roux, P. Schmitt, J. Kuchenbecker, B. Baradat, D. Lellouchi, C. Le-Touze, and J. M. Nicot, The advent of MEMS in space, Microelectron. Reliab. **43**, 1061 (2003).
[4] P. C. Lozano, B. L. Wardle, P. Moloney, and S. Rawal, Nanoengineered thrusters for the next giant leap in space exploration, MRS Bull. **40**, 842 (2015).
[5] J. J. Yao, C. Chien, R. Mihailovich, V. Panov, J. DeNatale, J. Studer, X. B. Li, A. H. Wang, and S. Park, Microelectromechanical system radio frequency switches in a picosatellite mission, Smart Mater. Struct. **10**, 1196 (2001).
[6] N. Kolhare, MEMS switches for 0.1–40 GHz for picosatellite application, Microsyst. Technol. **21**, 707 (2015).
[7] H. R. Shea, Radiation sensitivity of microelectromechanical system devices, J. Micro/Nanolithogr. MEMS MOEMS **8**, 031303 (2009).
[8] P. Schmitt, X. Lafontan, F. Pressecq, B. Kurz, C. Oudea, D. Esteve, J. Y. Fourniols, and H. Camon, Impact of the space environmental conditions on the reliability of a MEMS COTS based system, Microelectron. Reliab. **44**, 1739 (2004).
[9] C. H. Metzger and K. Karrai, Cavity cooling of a microlever, Nature (London) **432**, 1002 (2004).
[10] B. Lassagne, Y. Tarakanov, J. Kinaret, D. Garcia-Sanchez, and A. Bachtold, Coupling mechanics to charge transport in carbon nanotube mechanical resonators, Science **325**, 1107 (2009).
[11] L. Ding, C. Baker, P. Senellart, A. Lemaitre, S. Ducci, G. Leo, and I. Favero, High Frequency GaAs Nano-Optomechanical Disk Resonator, Phys. Rev. Lett. **105**, 263903 (2010).
[12] H. Okamoto, D. Ito, K. Onomitsu, H. Sanada, H. Gotoh, T. Sogawa, and H. Yamaguchi, Vibration Amplification, Damping, and Self-Oscillations in Micromechanical Resonators Induced by Optomechanical Coupling through Carrier Excitation, Phys. Rev. Lett. **106**, 036801 (2011).
[13] K. Usami, A. Naesby, T. Bagci, B. M. Nielsen, J. Liu, S. Stobbe, P. Lodahl, and E. S. Polzik, Optical cavity cooling of mechanical modes of a semiconductor nanomembrane, Nat. Phys. **8**, 168 (2012).
[14] T. Watanabe, H. Okamoto, K. Onomitsu, H. Gotoh, T. Sogawa, and H. Yamaguchi, Optomechanical photoabsorption spectroscopy of exciton states in GaAs, Appl. Phys. Lett. **101**, 082107 (2012).
[15] A. Reserbat-Plantey, L. Marty, O. Arcizet, N. Bendiab, and V. Bouchiat, A local optical probe for measuring motion and stress in a nanoelectromechanical system, Nat. Nanotechnol. **7**, 151 (2012).
[16] C. N. Arutt *et al.*, The study of radiation effects in emerging micro and nano electro mechanical systems (M and NEMS), Semicond. Sci. Technol. **32**, 013005 (2017).
[17] H. Q. Gong, W. J. Liao, E. X. Zhang, A. L. Sternberg, M. W. McCurdy, J. L. Davidson, R. A. Reed, D. M. Fleetwood,

R. D. Schrimpf, P. D. Shuvra, J. T. Lin, S. McNamara, K. M. Walsh, B. W. Alphenaar, and M. L. Alles, Total-ionizing-dose effects in piezoresistive micromachined cantilevers, IEEE Trans. Nucl. Sci. **64**, 263 (2017).

[18] R. W. Keyes, The electronic contribution to the elastic properties of germanium, IBM J. Res. Dev. **5**, 266 (1961).

[19] Y. Sun, S. E. Thompson, and T. Nishida, Physics of strain effects in semiconductors and metal-oxide-semiconductor field-effect transistors, J. Appl. Phys. **101**, 104503 (2007).

[20] A. Jaakkola, M. Prunnila, T. Pensala, J. Dekker, and P. Pekko, Determination of doping and temperature-dependent elastic constants of degenerately doped silicon from MEMS resonators, IEEE Trans. Ultrason. Ferroelectr. Freq. Control **61**, 1063 (2014).

[21] K. L. Ekinci and M. L. Roukes, Nanoelectromechanical systems, Rev. Sci. Instrum. **76**, 061101 (2005).

[22] P. D. Shuvra, S. McNamara, J. T. Lin, B. Alphenaar, K. Walsh, and J. Davidson, Axial asymmetry for improved sensitivity in MEMS piezoresistors, J. Micromech. Microeng. **26** (2016).

[23] Ariel Amir, Yuval Oreg, and Yoseph Imry, On relaxations and aging of various glasses, Proc. Natl. Acad. Sci. U.S.A. **109**, 1850 (2012).

[24] M. Razeghi and A. Rogalski, Semiconductor ultraviolet detectors, J. Appl. Phys. **79**, 7433 (1996).

[25] N. Shamir, J. G. Mihaychuk, and H. M. van Driel, Trapping and detrapping of electrons photoinjected from silicon to ultrathin SiO_2 overlayers in vacuum and in the presence of ambient oxygen, J. Appl. Phys. **88**, 896 (2000).

[26] J. Bloch, J. G. Mihaychuk, and H. M. van Driel, Electron Photoinjection from Silicon to Ultrathin SiO_2 Films via Ambient Oxygen, Phys. Rev. Lett. **77**, 920 (1996).

[27] B. H. Kang, W. P. Lee, H. K. Yow, and T. Y. Tou, Behaviour of total surface charge in SiO_2-Si system under short-pulsed ultraviolet irradiation cycles characterised by surface photo voltage technique, Appl. Surf. Sci. **255**, 6545 (2009).

[28] V. Fomenko and E. Borguet, Combined electron-hole dynamics at UV-irradiated ultrathin Si-SiO_2 interfaces probed by second harmonic generation, Phys. Rev. B **68**, 081301 (2003).

[29] Sanjay Banarjee and Ben G. Streetman, *Solid State Electronic Devices*, 6th ed. (Prentice Hall, Upper Saddle River, NJ, 2006), p. xviii.

[30] Y. C. Cheng and E. A. Sullivan, Effect of Coulomb scattering on silicon surface mobility, J. Appl. Phys. **45**, 187 (1974).

[31] Stephen D. Senturia, *Microsystem Design* (Kluwer Academic Publishers, Boston, 2001), p. xxvi.

[32] See Supplemental Material at http://link.aps.org/supplemental/10.1103/PhysRevApplied.8.034013 for calculations of the resonant frequency shift due to spring softening and surface absorbants.

[33] Raymond J. Roark, Warren C. Young, Richard G. Budynas, and Ali M. Sadegh, *Roark's Formulas for Stress and Strain*, 8th ed. (McGraw-Hill, New York, 2012), p. xviii.

[34] Robert W. Keyes, Electronic effects in the elastic properties of semiconductors, Solid State Phys. **20**, 37 (1968).

[35] P. Einspruch and N. G. Csavinszky, Effect of doping on the elastic constants of silicon, Phys. Rev. **132**, 2434 (1963).

[36] Ferdinand Pierre Beer, E. Russell Johnston, and John T. DeWolf, *Mechanics of Materials*, 4th ed. (McGraw-Hill Higher Education, Boston, 2006), p. xix.

[37] J. T. M. van Beek and R. Puers, A review of MEMS oscillators for frequency reference and timing applications, J. Micromech. Microeng. **22**, 013001 (2012).

[38] R. A. Kjar and D. K. Nichols, Radiation-induced surface states in MOS devices, IEEE Trans. Nucl. Sci. **22**, 2193 (1975).

[39] C. H. Qiu and J. I. Pankove, Deep levels and persistent photoconductivity in GaN thin films, Appl. Phys. Lett. **70**, 1983 (1997).

[40] R. Laiho, Y. P. Stepanov, M. P. Vlasenko, and L. S. Vlasenko, Persistent photoconductivity of ZnO, Physica (Amsterdam) **404B**, 4787 (2009).

[41] S. H. Choi, G. L. Park, C. C. Lee, and J. Jang, Persistent photoconductivity in hydrogenated amorphous-silicon, Solid State Commun. **59**, 177 (1986).

[42] P. Feng, I. Monch, S. Harazim, G. S. Huang, Y. F. Mei, and O. G. Schmidt, Giant persistent photoconductivity in rough silicon nanomembranes, Nano Lett. **9**, 3453 (2009).

[43] L. L. Zhu and X. J. Zheng, Modification of the elastic properties of nanostructures with surface charges in applied electric fields, Eur. J. Mech. A **29**, 337 (2010).

[44] S. T. Purcell, P. Vincent, C. Journet, and V. T. Binh, Tuning of Nanotube Mechanical Resonances by Electric Field Pulling, Phys. Rev. Lett. **89**, 276103 (2002).